Comparative assessment of the fate and toxicity of chemically and biologically synthesized silver nanoparticles to juvenile clams

Amar Y Al-Rshim [a,b], Jingjing Wang [a], Katy W. Chung [c], Frédéric Loosli [a], Anindya Chanda [a,d], Geoffrey I Scott [a], and Mohammed Baalousha [a*]

[a] Center for Environmental Nanoscience and Risk, Department of Environmental Health Sciences, Arnold School of Public Health, University of South Carolina, Columbia, SC, 29223, USA.

[b] Department of Marine Vertebrates, Marine Science Center, University of Basrah, Iraq.

[c] NOAA/National Ocean Service, Center for Coastal Environmental Health and Biomolecular Research, Charleston, SC, 29412, USA

[d] Mycologics LLC, Alexandria, VA, 22306, USA

* Corresponding Author

7837 words including abstract and references

5768 words including abstract and without references

5 figures

1 table

Abstract

Nanoparticles (NPs) can be produced via physical, chemical, or biological approaches. Yet, the impact of the synthesis approaches on the environmental fate and effects of NPs is poorly understood. Here, we synthesized AgNPs through chemical and biological approaches (cit-AgNPs and bio-AgNPs), characterized their properties, and toxicities relative to commercially available Ag nanopowder (np-AgNPs) to the clam *Mercenaria mercenaria*. The chemical synthesis is based on the reduction of ionic silver using sodium borohydride as a reducing agent and trisodium citrate as a capping agent. The biological synthesis is based on the reduction of ionic silver using biomolecules extracted from an atoxigenic strain of a filamentous fungus *Aspergillus parasiticus*. The properties of AgNPs were determined using UV-vis, dynamic light scattering, laser Doppler electrophoresis, (single particle)-inductively coupled plasma-atomic mass spectroscopy, transmission electron microscopy, and asymmetric flow-field flow fractionation. Both chemical and biological synthesis approaches generated spherical AgNPs. The chemical synthesis produced AgNPs with narrower size distributions than those generated through biological synthesis. The polydispersity of bio-AgNPs decreased with increases in cell free extract (CFE):Ag ratios. The magnitude of the zeta potential of the cit-AgNPs was higher than those of bio-AgNPs. All AgNPs formed aggregates in the test media *i.e.,* natural seawater. Based on the same total Ag concentrations, all AgNPs were less toxic than $AgNO_3$. The toxicity of AgNPs toward the juvenile clam, *Mercenaria mercenaria*, decreased following the order np-AgNPs > cit-AgNPs > bio-AgNPs. Expressed as a function of dissolved Ag concentrations, the toxicity of Ag decreased following the order cit-AgNPs > bio-AgNPs > $AgNO_3$ ~ np-AgNPs. Therefore, the toxicity of AgNP suspensions can be attributed to a combined effect of dissolved and particulate Ag forms. These results indicate AgNP synthesis methods determine their environmental and biological behaviors and should be considered for a more comprehensive environmental risk assessment of AgNPs.

1. Introduction

Silver nanoparticles (AgNPs) are the most widely used type of nanoparticles in consumer products [1]. AgNPs are used as antimicrobial agents, electrochemical sensors, biosensors, in medicine, health care, agriculture, and biotechnology [2, 3]. Silver nanoparticles (AgNPs) can be produced by two methods; that is "bottom-up" and "top-down". The bottom-up approach produces particles with better control on their physicochemical properties such as size, shape, surface charge, and colloidal stability [4]. The bottom-up synthesis of AgNPs can be achieved via chemical [5-7], physical [8-10], and biological [4, 11, 12] methods. The chemical synthesis of AgNPs in solution requires metal precursor (*e.g.,* $AgNO_3$), reducing agent (*e.g.,* ascorbic acid, alcohol, borohydride, sodium citrate, and hydrazine compounds), and stabilizing agent (*e.g.,* citrate, polyvinylpyrrolidone) [5-7]. Physical synthesis methods - such as arc-discharge [9], physical vapor condensation [8], energy ball milling methods [13], and direct current magnetron sputtering [10] – do not require highly reactive chemicals, but consume high energy [10]. Biosynthesis methods of AgNPs offer several advantages over chemical and physical synthesis as they are simple, cost-effective, eco-friendly, and can be scaled up for high yields and/or production [4, 14, 15].

Biosynthesis of AgNPs can be achieved inside (intracellular) or outside (extracellular) of biological organisms [16]. The extracellular synthesis of AgNPs is preferred over the intracellular synthesis because it is cheaper, favors large-scale production, and requires simpler downstream processing [17]. The intracellular synthesis requires additional steps to release the synthesized AgNPs such as ultrasound treatment or reactions with suitable detergents. Extracellular biological synthesis of AgNPs uses plants' or microorganisms' (*e.g.,* bacteria, fungi, and yeast) extracts as reducing and capping agents [4, 11, 12, 18-21]. Biomolecules secreted by plants (*e.g.,* carbohydrates, fats, proteins, nucleic acids, and secondary metabolites) and microorganisms (*e.g.,* enzymes, proteins, and bio-surfactants) serve as reducing agents to produce NPs from metal salts and capping agents to stabilize the synthesized NPs [18]. Filamentous fungi serve as a popular microbial source of biologically generated NPs including AgNPs [11, 17, 22-24]. AgNPs have been synthesized both intracellularly or extracellularly using filamentous fungi [23, 25-28] and the synthesized AgNPs are typically coated with proteins [28], carboxylic acid, unsaturated aldehydes, and

unsaturated alkaloids [29]. AgNPs have been synthesized using various fungus strains (**Table S1**) such as *Aspergillus foetidus* (20-40 nm) [30], *Aspergillus parasiticus* (less than 60 nm) [31, 32], *Aspergillus niger* (5–35 nm), and *Aspergillus terreus* (1–20 nm) [33].

Controlling the properties and stability of the synthesized AgNPs is essential for industrial production. The size, morphology, and stability of NPs depend on the method of preparation, nature of solvent, concentration, strength of reducing agent, and temperature [4, 11, 12, 34]. Optimization of the biosynthesis conditions - such as temperature, incubation time, extract concentration, and Ag concentration - is crucial to control the stability, size, and shape of the biosynthesized AgNPs [35-37]. However, the majority of previous studies focused on the biosynthesis of AgNPs under specific conditions without any attempt to control AgNP physicochemical properties. Only few studies performed systematic analysis of the impact of synthesis conditions on the properties of the synthesized AgNPs such as silver concentration, temperature, pH, reaction time, and concentration of cell extracts [24, 35, 38]. It is worth noting that the majority of studies reported the biosynthesis of polydispersed AgNPs [29, 39]. Additionally, the toxicity of AgNPs depends on their physicochemical properties such as size, shape, and surface coating, as well as, on their behavior (*i.e.* NPs stability and transformation) in the test medium such as dissolution and aggregation [40-44]. The toxicity of AgNPs could be attributed to the release of dissolved Ag [45], the particles themselves [46], or to the cumulative effect of AgNPs and dissolved Ag [47].

Although, several studies investigated the fabrication and characterization of AgNPs, including biosynthesis of AgNPs, few studies attempted to optimize the properties such as size and size distribution of the biosynthesized AgNPs, and/or compared their properties and toxicity to chemically synthesized and commercially available AgNPs. The aims of this study are to: **1)** biologically synthesize AgNPs (bio-AgNPs) with controlled sizes using cell free fungal secreted biomolecules, **2)** characterize the physicochemical properties of the synthesized AgNPs, and **3)** compare the toxicity of bio-AgNPs to juvenile clam *Mercenaria mercenaria* to that of chemically synthesized AgNPs (cit-AgNPs) and commercially available nanopowders (np-AgNPs).

2. Materials and Methods

2.1. Materials

Silver nitrate ($AgNO_3$) (ACS grade, 99.9+%), sodium borohydride ≥ 98.0% ($NaBH_4$) and a commercially available Ag-nanopowder (Nanopowder APS 20-40 nm, purity of ≥ 99.9% metals basis) were purchased from Alfa Aesar (Ward Hill, MA, USA). Trisodium citrate 99% ($Na_3C_6H_5O_7$) and sodium nitrate ($NaNO_3$) were purchased from VWR (West Chester, PA, USA). Trace metal grade nitric acid (68-70% HNO_3) and FL-70 were purchased from Fisher Scientific (Nazareth, PA, USA). Sodium azide was purchased from (Fisher Bioreagents™, India). Setup solution for inductively coupled plasma-mass spectrometer (ICP-MS) daily performance tuning was purchased from Perkin Elmer (Waltham, MA, USA). Internal standard and the silver (Ag) standard, manufactured by British Drug House (BDH chemicals, Randor, PA, USA), were purchased from VWR and were used to prepare standards for ICP-MS calibration. *Aspergillus parasiticus* strain AFS10 was obtained from Integrative Mycology Laboratory (IML) in the Department of Environmental Health Sciences (ENHS) within the Arnold School of Public Health (University of South Carolina, Columbia, SC, USA). Sucrose and Yeast Extract were supplied by VWR (Solon, OH, USA) and Thermo Fisher (Carlsbad, CA, USA), respectively. All solutions, suspensions, and media were prepared using ultrahigh purity water (UHPW, resistivity = 18.2 MΩ cm, Millipore Advantage System, Merck Millipore, Darmstadt, Germany). Prior to use, all plastic- and glassware were soaked using 10% v/v HNO_3 overnight, then rinsed in UHPW, followed by drying at room temperature. Natural seawater used to hold clams and to perform all exposures was collected from Belle W. Baruch Institute for Marine and Coastal Sciences, University of South Carolina. Crystal Seas® bioassay grade sea salts were purchased from the Marine Enterprises International, Baltimore, MD, USA.

The marine microalga *Isochrysis galbana* T-iso specimen (UTEX LB 987) was provided by Culture Collection of Algae, Department of Botany, University of Texas at Austin (UTEX) and used as a food source for juvenile clams in toxicity tests. The Juvenile clams, *Mercenaria mercenaria*, of approximately 0.820 – 1.2 mm in size were purchased from Bay Shellfish Inc. (Terra Ceia, FL, USA). The clams were shipped overnight in a mesh netting. Upon arrival at the laboratory, the clams were placed in a glass finger

bowl (approx. 1.5 L) and rinsed with fresh 20-psu (practical salinity unit) seawater at least 3 times to wash off any debris. The clams were sieved using a 0.85-mm sieve. The sizes of the retained clams ranged 0.85–1.28 mm and averaged 1.2 mm. The separated clams were then acclimated for 7 days prior to toxicity assays in 600-mL pre-cleaned glass beaker under standard lab holding conditions: 20 ºC, 20-psu, 16/8h light/dark cycle, gentle aeration using air-stone attached to an airline, daily feeding using 50 ml of *Isochrysis galbana* (average count of 6-8 million cells/mL), and daily replacement of ¾ of the total seawater volume to minimize ammonia concentration.

2.2. Silver nanoparticles

Three types of AgNPs were used in this study, including chemically synthesized (cit-AgNPs), biologically synthesized (bio-AgNPs), and commercially available silver nanopowder (np-AgNPs). A schematic representation of the cit-AgNP and bio-AgBP synthesis, as well as the npAgNP dispersion is presented in **Figure 1**. Citrate-stabilized silver nanoparticle (cit-AgNPs) were synthesized using hydrothermal synthesis approaches under sterile conditions as described elsewhere [48-50]. Briefly, cit-AgNPs were synthesized by reducing ionic silver using sodium borohydride ($NaBH_4$) in the presence of trisodium citrate ($Na_3C_6H_5O_7$). Solutions of 1.69 mL of 58.8 mM silver nitrate, and 2.92 mL of 34 mM trisodium citrate dihydrate were added to 400 mL of boiling water while vigorously stirring at 600 rpm (VWR® Advanced Hot Plate Stirrer, Henry Troemner, LLC., NJ, USA), followed by adding 2.0 mL of 100 mM sodium borohydride into mixture dropwise while stirring for another 15 minutes. The hotplate was turned off and the resulting suspension was left for 45 min on a hot plate, and then left overnight at ambient temperature. The final product was stored in the dark at 4°C.

Bio-AgNPs were synthesized using the cell free filtered extracts of an atoxigenic *Aspergillus parasiticus* strain AFS10[51] as reducing and capping agents. To prepare biomass for biosynthesis, the fungi were grown in a liquid growth media, YES (containing 2% w/v yeast extract, 6% w/v sucrose; pH 5.8). A total of 10^5 spores mL^{-1} was inoculated, and the growth medium was incubated in the dark on an orbital shaker at 29°C and agitated at 150 rpm. The biomass was harvested after 48-h of growth by filtration using a Mira cloth, followed by extensive washing with autoclaved UHPW to remove any medium

153 component from the biomass. Then, 20 g of biomass (fresh weight) was introduced into 200 ml of UHPW
154 for 72-h at 29°C in an Erlenmeyer flask and agitated under the same condition as described earlier. The cell
155 free extract composed of secreted fungal biomolecules in UHPW was isolated from the cells using filtration
156 with Mira cloth. For biological synthesis of AgNPs, 1 mM $AgNO_3$ solution was mixed with cell free extract
157 solution at CFE:Ag^+ ratios of 1:10, 1:5, 1:1, 5:1, 10:1, 25:1, and 50:1 by volume in a 250-ml Erlenmeyer
158 flask and agitated at 60°C in the dark. The formation/growth of bio-AgNPs was monitored by measuring
159 the changes in the surface Plasmon resonance over time using a dual beam UV absorbance spectrometer
160 (UV-vis) (Shimadzu UV-2600 spectrophotometer, Shimadzu Co., Kyoto, Japan) using cuvettes with 10
161 mm optical path length.

162 Excess reactants in the synthesized solution were removed by diafiltration under high pressure in
163 the presence of N_2 using stirred-cell ultrafiltration (Amicon, 3-KDa regenerated cellulose membrane,
164 Millipore, MA, USA) [48, 49]. AgNP suspension volume was reduced by half and then replenished by
165 adding an equivalent volume of 0.25 mM sodium citrate solution for the cit-AgNPs and ultrapure water for
166 bio-AgNPs. This process was repeated five times to ensure the removal of the majority of unconsumed
167 reactants. The cleaned AgNP suspensions were filtered through a 0.45 μm cellulose nitrate membrane
168 (Millipor, Billerica, MA, USA) using a Millipore Inc. filtration flask and funnel to eliminate any large NP
169 aggregates that may have formed during the synthesis.

170 Commercially available silver nanopowder (np-AgNPs) was suspended in UHPW at a
171 concentration of 1000 μg L^{-1}, followed by vigorous stirring for 30 min at 1000 rpm at room temperature.
172 Then the suspension was ultra-sonicated for 3 hours in an ice-bath (Branson 2800 ultrasonic cleaner,
173 Danbury, CT, USA) to enhance the disaggregation of AgNP aggregates. The sonicated AgNP suspension
174 was stirred for 24 h and then centrifuged for 5 min at 3500 rpm using Thermo Scientific centrifuge (Legend
175 RT Plus, Thermo Electron Co., Waltham, MA, USA) to remove AgNP aggregates larger than 200 nm. The
176 supernatant was collected and kept in dark at 4°C until use.

177 **2.3. Physicochemical properties of AgNPs**

Total Ag concentrations of AgNP stock suspensions were determined using ICP-MS (NexION 350D, PerkinElmer Inc., Waltham, MA, USA). Prior to ICP-MS analysis, AgNPs were digested in nitric acid (HNO_3, trace metal grade 68-70%) at room temperature overnight and then diluted 200-fold in 1% HNO_3. The ICP-MS measurement conditions were optimized daily using the setup solution to achieve high sensitivity with limited interferences. A calibration curve was produced using a series of ionic silver standards (0.0, 0.1, 0.5, 1.0, 5, and 10 μg L^{-1}) prepared in 1% nitric acid (Trace Metal grade, Fisher Chemicals, Fair Lawn, NJ, USA). Indium (^{115}In) was added to samples and standards to be monitored as an internal standard to correct for non-spectral interferences during the analysis.

The z-average hydrodynamic diameter of AgNPs was determined using dynamic light scattering (DLS) (Nano-ZS, Malvern Instruments Ltd., Malvern, UK) and was reported as the mean and standard deviation of five independent replicates. The mass weighted hydrodynamic diameter (d_H) was determined using asymmetrical flow field-flow fractionation (AF4, DualTec Eclipse, Wyatt Technology, Santa Barbara, CA, USA) coupled to ICP-MS (Perkin Elmer NexION350D) as described in detail elsewhere [52]. The AF4 was equipped with 350 μm spacer and a 1-kDa Pall Omega polyethersulfonate membrane (Pall Corporation, Port Washington, NY, USA). The AF4 carrier solution consisted of 10 mM $NaNO_3$, 0.01% sodium azide, and 0.0125% FL-70 in UHPW. Particle fractionation was performed by applying a constant cross and detector flows of 1.0 mL min^{-1}. The AF4 channel was calibrated using Latex nanosphere size standards of 20, 40, 80, and 150 nm prior to sample analysis (Thermo Scientific, Fermont, CA, USA). All samples were bath sonicated for 15 min and 5 μL was injected into the AF4 channel for size fractionation. The fractionated particles were then transported to the ICP-MS for elemental analysis by connecting the AF4 outlet line to a Y-connector (PEEK, Analytical Sales & Services, Flanders, NJ, United States), through which a constant 10 μg L^{-1} internal standard in 2 % nitric acid (Trace Metal Grade, Fisher Chemical, Fair Lawn, NJ, United States) was introduced to monitor and correct any possible signal drift over time.

Particle core diameter was determined using single particle ICP-MS (SP-ICP-MS) as described in detail elsewhere [52]. Briefly, SP-ICP-MS analysis was performed using a Perkin Elmer NexION350D with Syngistix 1.0 in Nano application module. The instrument was tuned in the same way as for

conventional ICP-MS analysis. The transport efficiency was determined before sample analysis by analyzing a series of dissolved Au standards (0, 5, 10, and 20 µg L^{-1}, diluted in 1% HCl, BDH Chemicals, West Chester, PA, USA) and an Au nanoparticle standard (NIST™ 8013, diluted 10^5 times, Gaithersburg, MD, USA) [53]. Ionic Ag standard solutions were prepared by diluting commercial standards (Ag, Ricca, Arlington, TX, USA) to 5, 10, and 20 µg L^{-1} in 1% HNO_3. ^{107}Ag was monitored with a 50 µs dwell time, and 60 s acquisition time. All samples were diluted 100 folds to avoid coincidence and to minimize background signal. A rinse cycle consisting of 1 min with 1% HNO_3 was performed after each sample run to eliminate interferences between samples. SP-ICP-MS measures particle mass, from which the particle diameter can be calculated assuming a single spherical particle. All samples were prepared and analyzed in triplicates and all data are presented as the mean and standard deviation of three independent replicate measurements.

Particle core diameter and morphology were determined using a H-7800 transmission electron microscopy (TEM, Hitachi, Tokyo, Japan) with an acceleration voltage of 200 keV. For TEM analysis, AgNP stock suspensions were pipetted onto carbon-coated 50 mesh Cu grids (S162-3, AGAR Scientific, location), and allowed to adsorb to the carbon coating for 15 min followed by rinsing with UHPW to remove unadsorbed particles. Subsequently, the grids were left to dry for 48 h in a covered petri dish at room temperature. The particle diameters were determined using ImageJ (Release 152a, National Institutes of Health, Bethesda, MD, USA) and all data are presented as mean ± standard deviation of the particle size distribution.

The electrophoretic mobility was determined using laser Doppler electrophoresis, which was used to calculate the zeta potential (ζ) using Smoluchowski's assumption [54]. The zeta potential (ζ) was reported as the mean and standard deviation of ten replicates.

The dissolved Ag concentration in the bioassay exposure medium (20-psu seawater) was separated by centrifugal ultrafiltration (3 KDa regenerated cellulose membranes, Amicon Ultra-4, MA, USA). Four mL aliquots of exposure medium containing Ag ($AgNO_3$, cit-AgNPs, bio-AgNPs, or np-AgNPs) from the different bioassays were collected at 0 and 24 h and were centrifuged for 20 min at 4000 rpm using an

Eppendorf 5810R centrifuge (Hamburg, Germany). The filtrate was acidified to 1% of HNO_3 and were analyzed by ICP-MS as described above. The aggregation of AgNPs in the bioassay exposure medium was monitored by measuring the z-average hydrodynamic diameter of AgNPs using DLS as described above.

2.4. Biological assays

2.4.1. Algae culture

Artificial Seawater (ASW), used for algae culture, was prepared by dissolving Crystal Seas® bioassay grade sea salts in UHPW until a salinity of 28.5–30.5 psu was measured. The resulting solution was aerated to achieve O_2 saturation > 90% and was then filtered twice using 0.45 µm cellulose nitrate membrane filter (VWR® Millipore Inc., Buckinghamshire, UK). The pH of the ASW was 8.1 ± 0.1 throughout in all bioassays study. *Isochrysis galbana* was cultivated in standard F/2 (Guillard's) medium (**Table S3**) using artificial seawater (ASW) in 500-mL sterilized flasks containing 300 mL sterile media and 10% (v/v) algal inoculum. Flasks were maintained without aeration at 24°C, with constant illumination of 16:8 hours light:dark conditions using white cool fluorescent lamps on an orbital shaker at 100 rpm. Then, 5 to 7 days later, the algal culture was transferred into 2 L-glass bottles. Algae were concentrated by centrifugation at 3,500 rpm for 20 minutes (Beckman model Allegra X-12R, Ramsey, MN, USA) prior to daily feeding of clams.

2.4.2. Acute clam *Mercenaria mercenaria* toxicity test

The acute toxicity of silver (ionic and NP forms) to juvenile clam, *M. mercenaria,* was assessed in aqueous bioassays. First, a range finder test was performed for each Ag form ($AgNO_3$, cit-AgNPs, bio-AgNPs, and np-AgNPs) separately using a series of Ag concentrations to determine the most appropriate Ag concentrations for the determination of the LC_{50}, which was found to be 180 to 380 µg-Ag L^{-1} for $AgNO_3$ and 200 to 2600 µg-Ag L^{-1} for AgNPs. Then, the 24-h acute toxicity (mortality) was assessed by exposing ten clams/replicate (5 replicates/exposure concentration) to $AgNO_3$, cit-AgNPs, bio-AgNPs, and np-AgNPs in static non-renewal tests in 600-mL glass beakers filled with 300 mL natural seawater at 20-psu salinity, 25°C, a 16-h light: 8-h dark cycle, and without feeding. The nominal dissolved Ag exposure concentrations were 180, 220, 260, 300, 340, and 380 µg-Ag L^{-1}. The nominal AgNP exposure

concentrations were 0.00, 200, 350, 600, 1000, 1500, and 2600 µg-Ag L^{-1}. Water quality parameters (Oxygen saturation ≥ 78%, temperature 22-23°C, salinity 20.09 ± 0.13 psu, and pH 8 ± 0.15) were measured in select replicates for each Ag test concentration and the controls, using YSI professional plus multiparameter instrument (YSI Incorporated, OH, USA). At the end of the exposure period (24 h), the mortality of juvenile clams were determined by observing the gaping of valves and lack of locomotion under an Olympus SZH10 Microscope (Olympus optical, Ltd. Tokyo, Japan) at 7.0× magnification. The bioassays were rejected if the control mortality was >10%. The median lethal concentration (LC_{50}, µg L^{-1}) and the corresponding 95% confidence limits (CL) were determined for each bioassay using the Trimmed Spearman–Karber method [55]. Analysis of variance (ANOVA) with Dunnett's procedure was used to determine if the mean mortality was different among the different treatments ($p < 0.05$). All statistical analyses were performed using SAS version 9.4 software (SAS® Institute, Cary, NC, USA). The no observable effect concentration (NOEC) was determined as the highest nominal test concentration that had no statistically significant mortality, and the lowest observed effect concentration (LOEC) was determined as the lowest nominal test concentration that had statistically significant mortality, were calculated [56].

Sodium dodecyl sulfate (SDS) was used as a reference toxicant to ensure that the clams used in the bioassays were healthy. Ten clams were placed in 600-ml beaker containing seawater and 0, 1940, 3240, 5400, 9000, 15000 and 25000 µg L^{-1} SDS. The population of juvenile clams was considered healthy if the SDS LC_{50} was within two standard deviations of the average LC_{50} of 6740 to 9270 µg L^{-1}.

3. Results and discussion

3.1. Properties of AgNPs

The color of $AgNO_3$ solution changed from colorless to yellow and brown for chemical and biological synthesis methods, respectively, providing initial evidence of the reduction of Ag^+ to Ag^0 and the formation of AgNPs (**Figure S1**). The color intensity of the biologically synthesized AgNPs increased with increases in CFE:Ag^+ ratio indicating the increased concentration of the formed AgNPs. Three absorption bands were

identified in the UV-vis absorption spectra of cit-AgNPs and bio-AgNPs at 220, 270, and 390 or 430 to 435 nm (**Figure S2**). The absorption band at 220 nm has been attributed to absorption by amide bond and the absorption band at 270 nm has been attributed to electronic excitations in tryptophan and tyrosine residues present in the protein [57]. This observation suggests the release of proteins into the medium by *A. parasiticus* which act as a reducing agent that converts Ag^{+} to Ag^{0}, resulting in the formation of AgNPs [58, 59]. These proteins bind to the AgNP surfaces - *via* covalent bonds between functional groups (*e.g.,* the amino groups and cysteine residues) and AgNP surfaces and/or electrostatic interactions between carboxyl groups and AgNP surfaces - and enhance AgNP colloidal stability [58-61]. The intensity of the Plasmon resonance at 220 and 270 nm increased with increases in CFE:Ag^{+} ratio due to increases in protein concentrations. The absorption band at 390 and 430 to 435 nm are attributed to the formation of AgNPs for cit-AgNPs and bio-AgNPs, respectively. The majority of bio-AgNPs reported in the literature display a Plasmon resonance peak between 405 and 450 nm (**Table S1**). The higher Plasmon resonance peak position of bio-AgNPs compared to cit-AgNPs can be attributed to the formation of larger particles or to changes in AgNPs surface chemistry due to differences in the nature of the surface coating (*e.g.,* protein *vs.* citrate). The surface Plasmon resonance arise from the coherent oscillations of conduction band electrons near the NP surfaces. The surface Plasmon resonance peak position of AgNPs depends on the nature of the interactions between the Ag surface atoms and the surface coating and the thickness of the surface coating [62]. The surface Plasmon resonance peak position of AgNPs increases (red shift) with increases in the bond strength between the Ag surface atoms and the molecules forming the surface coating as well as the thickness of the surface coating [62]. Such red shifts in the surface Plasmon resonance of AgNPs have been attributed to the reduction of the conduction band electrons when the anchor group of the surface coating molecules is modified [62]. The formation of covalent bonds with amines and thiols (*e.g.,* Ag-N, Ag-S) reduces the density of the conduction band electrons in the surface by 36.8 and 45.2 %, respectively, in comparison with that of the bulk Ag [63]. On the other hand, citrate ions interact with AgNP surface via multiple carboxylate groups (*e.g.,* Ag-O) of the citrate molecule resulting in a weaker bonds compared to those formed between AgNP surfaces and proteins [64]. The UV-vis absorbance intensity of bio-AgNPs

307 increased with increases in CFE:Ag^+ ratios due to the increased concentrations of proteins in the CFE as
308 indicated by the increase in UV-vis absorbance at 220 and 280 nm. Bio-AgNP suspensions display broader
309 absorption bands compared to the narrow absorption bands of cit-AgNPs (**Figure S2**). This is likely due to
310 higher polydispersity of bio-AgNPs and diversity of molecules that form bio-AgNP surface coating [62].
311 The absorbance intensity at maximum absorption wavelength of AgNPs increased with increases in
312 CFE:Ag^+ ratio and reaction time, indicating increased yield of AgNPs (**Figure S3a**). The intensity of UV-
313 vis absorption at 120 h increased with increases in CFE:Ag^+ ratios and then plateaued at CFE:Ag^+ of 10:1,
314 indicating that the minimum amount of CFE extracts required to reduce the majority of Ag^+ under the
315 experimental conditions (**Figure S3a**).

316 The z-average hydrodynamic diameter (d_H) of cit-AgNP and bio-AgNPs, measured by DLS, illustrates
317 that cit-AgNPs exhibit the smallest size and the narrowest particle size distribution with the smallest
318 polydispersity index (PdI) value compared to bio-AgNPs (**Table 1**). The z-average hydrodynamic diameter
319 of the bio-AgNPs generally decrease with increases in CFE:Ag^+ ratio. The PdI of the bio-AgNPs decreased
320 with increases in CFE:Ag^+, with the bio-AgNPs at CFE:Ag^+ ratio of 50:1 exhibiting the smallest size and
321 narrowest particle size distribution with the smallest PdI (**Table 1**). AF4 fractograms of cit- and bio-AgNPs
322 are presented in **Figure 2a**. The cit-AgNPs and bio-AgNPs (CFE:Ag 50:1, 25:1, and 10:1) display
323 monomodal size distributions. Conversely, bio-AgNPs (CFE:Ag^+ of 5:1, 1:1, 1:5, and 1:10) display broad
324 bimodal size distributions. These results are in good agreement with the trend of the z-average
325 hydrodynamic diameters and PdIs measured by DLS. These results indicate the decreased polydispersity
326 of bio-AgNPs with increases in CFE:Ag^+ ratios.

327 TEM micrographs and the corresponding number particle size distributions of AgNPs are presented in
328 **Figure 3**. TEM micrographs illustrate that both chemical and biological synthesis result in the formation
329 of spherical AgNPs (**Figure 3a and b**). The mean core diameter of the cit-, bio- and np-AgNPs were ca 9.7
330 ± 3.5, 15.9 ± 6.0, and 74.1 ± 19.7, respectively (**Table 1**). Both cit-AgNPs and bio-AgNPs exhibit spherical
331 shapes and dispersed NP suspensions without clusters or aggregates. Conversely, np-AgNPs exhibit
332 irregular shapes and the formation of AgNP aggregates (**Figure 3c**).

The mean sizes of AgNPs measured by the four different techniques (**Table 1**) follow the order DLS > AF4-ICP-MS > SP-ICP-MS > TEM. This is because these analytical techniques use different measurement principles, provide different measures of NP size, and different weighting of the particle size distribution [5, 65]. DLS and AF4-ICP-MS measure NP hydrodynamic diameter (*i.e.,* core size + diffuse layer) whereas TEM, and SP-ICP-MS measure particle core size. Thus, the NP sizes measured by DLS and AF4-ICP-MS are generally larger than those measured by TEM, and SP-ICP-MS. The higher hydrodynamic diameter measured by DLS compared to AF4-ICP-MS is because DLS measures the intensity-based particle size distribution (PSD) whereas AF4-ICP-MS measures mass-based PSD. The larger core diameters measured by SP-ICP-MS compared to TEM are due to the high mass (size) detection limit of SP-ICP-MS (*e.g.,* 15 nm), resulting in the overestimation of AgNP core diameter by SP-ICP-MS. The difference between the hydrodynamic diameter measured by AF4-ICP-MS and the core diameter measure by TEM also is partially attributed to the thickness of the surface coating. Such a difference is greater for bio-AgNPs than for cit-AgNPs, indicating the formation of a thicker surface coating on bio-AgNPs than on cit-AgNPs.

The zeta potential (ζ) of AgNPs is presented in **Table 1**. Cit-AgNPs and bio-AgNPs (CFE:Ag^+ ratios of 50:1) display the highest zeta potential magnitude of 42.1 ± 1.6 and 42.0 ± 1.1 mV, respectively. The magnitude of zeta potential of bio-AgNPs increased with increases in CFE:Ag^+ ratios, which can be attributed to the increased surface coating of bio-AgNPs with biomolecules which imparts a higher surface charge, which in turn results in increased AgNP surface charge and colloidal stability. Zeta potential is generally correlated with NP colloidal stability where, as a rule of thumb, zeta potentials of lower than -30 mV of greater than +30 mV indicate NPs colloidal stability of charge (electrostatically) stabilized NPs [66, 67].

All AgNPs formed aggregates in seawater and the aggregate size increased with time (**Figure 4**). Aggregate size increased following the order bio-AgNPs <~ cit-AgNPs < np-AgNPs. This is in good agreement with the higher zeta potential magnitude of cit-AgNPs and bio-AgNPs compared to np-AgNPs. This is also in agreement with the increased thickness of the surface coating of bio-AgNPs than cit-AgNPs.

In the exposure medium (*e.g.,* natural seawater), the total Ag concentrations measured at the beginning of the bioassay were in good agreement with the nominal concentrations (**Figure S4**). However, at the end of the exposure (24 h), the measured Ag concentrations were lower than nominal concentrations. This is likely due to losses of AgNPs from the suspension as a result of aggregation (**Figure 4**) and sedimentation. The decrease in the total Ag concentration was higher for np-AgNPs than for cit-AgNPs and bio-AgNPs, in agreement with the larger aggregate size of np-AhNPs compared to cit-AgNPs and bio-AgNPs (**Figure 4**).

The concentrations of total and dissolved Ag were not significantly different during $AgNO_3$ exposure (**Figure 5a**). At the beginning of the exposure (t = 0 h), the concentration of dissolved Ag increased with increases in total Ag concentration and decreased following the order $AgNO_3$ > np-AgNPs > cit-AgNPs >~ bio-AgNPs (**Figure 5a**). At the end of the exposure (t = 24 h), the dissolved Ag concentration in cit-AgNPs and bio-AgNP suspensions were slightly higher than those measured at the beginning of the exposure (**Figure 5b**). In contrast, the dissolved Ag concentration in np-AgNP suspension at the end of the exposure was much higher than those measured at the beginning of the exposure and exceeded the dissolved Ag concentration from $AgNO_3$ (**Figure 5b**). Bared AgNPs are more susceptible to dissolution than coated NPs because surface coating can act as a barrier between the nanoparticle surfaces and the environment and consequently hinder the oxidation of AgNP surfaces. Biomolecule coating may prevent/reduce the dissolution of AgNPs to a higher extent than citrate because biomolecules form a thicker surface coating and contain reducing moieties that may counteract the oxidative dissolution of AgNPs [68].

3.3. Toxicity of the AgNPs

Clam survival in the controls was > 96% in all assays. The LC_{50} of the reference toxicant (SDS exposure) ranged from 6740 to 9270 µg L^{-1}. These LC_{50} values are within the acceptable range and thus all batches of clams were determined to be healthy (**Table S4**). The dose-response curves of clams exposed to $AgNO_3$, cit-AgNPs, bio-AgNPs, and np-AgNPs show that all forms of Ag induced juvenile clams' mortality (**Figure 6a**). The mortality of the juvenile clams increased with increases in total Ag concentration for the different forms of Ag. The mortality of the juvenile clams based on total Ag–exposure concentration

indicated that the toxicity of Ag species decreased following the order $AgNO_3$> np-AgNPs > cit-AgNPs > bio-AgNPs. The LC_{50} increased following the order of 240 µg L^{-1} $AgNO_3$ (95% CI: 220–270 µg L^{-1}) < 700 µg L^{-1} np-AgNPs (95% CI: 640–870 µg L^{-1}) < 1050 µg L^{-1} cit-AgNPs (95% CI: 900–1360 µg L^{-1}) < 2440 µg L^{-1} bio-AgNPs (95% CI: 1810–2430 µg L^{-1}) (**Table S5**). The NOEC of $AgNO_3$, np-AgNPs, cit-AgNPs, and bio-AgNPs were 0.00, 200, 200, and 350 µg L^{-1}, respectively and the LOEC were 180, 350, 600, and 1000 µg L^{-1} respectively (**Table S5**). Some previous studies attributed the toxicity of AgNP suspensions to the release of dissolved Ag only [69, 70], while others attributed the toxicity of AgNP suspensions to particle-specific effects in addition to dissolved Ag effect [71, 72], and others attributed the toxicity of AgNPs predominantly to particle-specific effects [73].

The mortality of the juvenile clams based on the measured dissolved Ag exposure concentrations indicated that the toxicity of Ag chemical species followed the order cit-AgNPs ~ bio-AgNPs > $AgNO_3$ > np-AgNPs after 24h of exposure (**Figure 6b**). The LC_{50} (in µg L^{-1}) decreased following the order of cit-AgNPs 96.8 (95% CI: 70 – 133) ~ bio-AgNPs 100 (95% CI: 70.4 – 140) < $AgNO_3$ 240 (95% CI: 220 – 270) < np-AgNPs 248.6 (95% CI: 185 – 334) (**Table S5**). The NOEC of $AgNO_3$, np-AgNPs, cit-AgNPs, and bio-AgNPs were 0.00, 200, 200, and 350 µg. L^{-1}, respectively and the LOEC were 180, 350, 600, and 1000 µg. L^{-1} respectively (**Table S5**). Expressing the mortality of the juvenile clams as a function of dissolved Ag at t = 24 h indicates that dissolved Ag explains the toxicity of np-AgNPs, which dissolved to a higher extent than cit-AgNPs and bio-AgNPs (**Figure 5b**). However, dissolved Ag does not fully explain the differences in the toxicity of cit-AgNP and bio-AgNP suspensions, indicating that the toxicity of cit-AgNP and bio-AgNP suspensions can be attributed to both dissolved and particulate Ag forms. Overall, these results indicate AgNPs possess intrinsic toxic effects and that dissolved Ag explains only a portion of the toxicity of AgNP suspensions primarily when the dissolution of AgNPs is excessive. These results are in agreement with previous studies which demonstrated that the released silver ions and particulate Ag contribute to the toxicity of AgNPs to organisms such as earthworm Eisenia fetida [74] and fungus *Phanerochaete chrysosporium* [75].

4. Conclusions

This study demonstrated the synthesis of AgNPs with similar physicochemical properties (*e.g.,* size, shape, and zeta potential) via chemical and biological approaches. The chemical synthesis is based on reducing ionic silver using sodium borohydride in the presence of trisodium citrate as a capping agent. The biological approach is based on the use of cell-free extracts of AFS10 as reducing and capping agents to convert ionic silver to metallic silver and to impart AgNP stability. Higher CFE:Ag^{+} ratios resulted in higher AgNP yields and narrower size distributions. The smallest bio-AgNPs were characterized by similar size distribution as those generated through chemical synthesis (cit-AgNPs). Both chemical and biological synthesis approaches resulted in the formation of spherical AgNPs. The chemical synthesis approach generated AgNPs with a lower size polydispersity compared to the biological synthesis approach.

This study also compared the fate and toxicity of chemically- and biologically synthesized AgNPs alongside silver nanopowder (np-AgNPs) and silver nitrate ($AgNO_3$) to juvenile hard clams (*Mercenaria mercenaria*), which are a commercially important species. All AgNPs formed aggregates in seawater and the size of these aggregates decreased following the order np-AgNPs > cit-AgNPs > bio-AgNPs. Additionally, all AgNPs underwent dissolution in seawater and the concentration of dissolved Ag decreased following the order np-AgNPs > cit-AgNPs > bio-AgNPs. Furthermore, this study demonstrated that both dissolved and nanoparticulate Ag induce toxicity to the juvenile clam, *M. mercenaria*, which decreased following the order (based on total Ag concentration) $AgNO_3$ > np-AgNPs > cit-AgNPs > bio-AgNPs. The toxicity of AgNP suspensions could not be fully explained by the dissolved Ag concentrations, and is thus, attributed to both dissolved Ag and nanoparticulate Ag. Overall, this study illustrated that the synthesis route could affect the environmental fate and effects of AgNPs, which should be taken into account in risk assessment of AgNPs. From a perspective of fate and toxicity, due to their low dissolution and toxicity, bio-AgNPs are recommended over the cit-AgNP and np-AgNPs.

Acknowledgment

This research was supported by the Iraqi Ministry of Higher Education and Scientific Research (MOHESR) and the United States National Science Foundation (NSF1437307).

[1] F. Piccinno, F. Gottschalk, S. Seeger, B. Nowack, Industrial production quantities and uses of ten engineered nanomaterials in Europe and the world, J Nanopart Res J.Nanopart.Res., Springer Netherlands, 2012, pp. 1-11.
[2] S. Torkamani, S. Wani, Y. Tang, R. Sureshkumar, Plasmon-enhanced microalgal growth in miniphotobioreactors, Applied physics letters, 97 (2010) 043703.
[3] N. Gong, K. Shao, W. Feng, Z. Lin, C. Liang, Y. Sun, Biotoxicity of nickel oxide nanoparticles and bio-remediation by microalgae Chlorella vulgaris, Chemosphere, 83 (2011) 510-516.
[4] A. Husen, K.S. Siddiqi, Phytosynthesis of nanoparticles: concept, controversy and application, Nanoscale research letters, 9 (2014) 1-24.
[5] M. Baalousha, J.R. Lead, Rationalizing Nanomaterial Sizes Measured by Atomic Force Microscopy, Flow Field-Flow Fractionation, and Dynamic Light Scattering: Sample Preparation, Polydispersity, and Particle Structure, Environ. Sci. Technol, 46 (2012) 6134-6142.
[6] Q. Zhang, N. Li, J. Goebl, Z. Lu, Y. Yin, A systematic study of the synthesis of silver nanoplates: is citrate a “magic” reagent?, Journal of the American Chemical Society, 133 (2011) 18931-18939.
[7] G.A. Sotiriou, S.E. Pratsinis, Antibacterial activity of nanosilver ions and particles, Environmental science & technology, 44 (2010) 5649-5654.
[8] K.M. Abou El-Nour, A.a. Eftaiha, A. Al-Warthan, R.A. Ammar, Synthesis and applications of silver nanoparticles, Arabian journal of chemistry, 3 (2010) 135-140.
[9] D.-C. Tien, K.-H. Tseng, C.-Y. Liao, J.-C. Huang, T.-T. Tsung, Discovery of ionic silver in silver nanoparticle suspension fabricated by arc discharge method, Journal of alloys and compounds, 463 (2008) 408-411.
[10] P. Asanithi, S. Chaiyakun, P. Limsuwan, Growth of silver nanoparticles by DC magnetron sputtering, Journal of Nanomaterials, 2012 (2012).
[11] K.S. Siddiqi, A. Husen, Fabrication of metal nanoparticles from fungi and metal salts: scope and application, Nanoscale research letters, 11 (2016) 1-15.
[12] K.S. Siddiqi, A. Husen, Fabrication of metal and metal oxide nanoparticles by algae and their toxic effects, Nanoscale research letters, 11 (2016) 1-11.
[13] A. Kosmala, R. Wright, Q. Zhang, P. Kirby, Synthesis of silver nano particles and fabrication of aqueous Ag inks for inkjet printing, Materials Chemistry and Physics, 129 (2011) 1075-1080.
[14] A. Husen, K.S. Siddiqi, Plants and microbes assisted selenium nanoparticles: characterization and application, Journal of nanobiotechnology, 12 (2014) 1-10.
[15] K.S. Siddiqi, A. Husen, Green synthesis, characterization and uses of palladium/platinum nanoparticles, Nanoscale research letters, 11 (2016) 1-13.
[16] A. Saravanan, P.S. Kumar, S. Karishma, D.-V.N. Vo, S. Jeevanantham, P.R. Yaashikaa, C.S. George, A review on biosynthesis of metal nanoparticles and its environmental applications, Chemosphere, 264 (2021) 128580.
[17] N. Duran, P. Marcato, O. Alves, G. De Souza, E. Esposito, Mechanistic aspects of biosynthesis of silver nanoparticles by several Fusarium oxysporum strains, J. Nanobiotechnol, 3 (2005) 8.
[18] K.S. Siddiqi, A. Husen, R.A.K. Rao, A review on biosynthesis of silver nanoparticles and their biocidal properties, Journal of Nanobiotechnology, 16 (2018) 14.
[19] A.R. Shahverdi, S. Minaeian, H.R. Shahverdi, H. Jamalifar, A.-A. Nohi, Rapid synthesis of silver nanoparticles using culture supernatants of Enterobacteria: a novel biological approach, Process Biochemistry, 42 (2007) 919-923.
[20] N. Saifuddin, C.W. Wong, A.A. Yasumira, Rapid biosynthesis of silver nanoparticles using culture supernatant of bacteria with microwave irradiation, E-journal of Chemistry, 6 (2009) 61-70.
[21] S. Lokina, A. Stephen, V. Kaviyarasan, C. Arulvasu, V. Narayanan, Cytotoxicity and antimicrobial activities of green synthesized silver nanoparticles, European journal of medicinal chemistry, 76 (2014) 256-263.

[22] A. Ingle, A. Gade, S. Pierrat, C. Sonnichsen, M. Rai, Mycosynthesis of silver nanoparticles using the fungus Fusarium acuminatum and its activity against some human pathogenic bacteria, Current Nanoscience, 4 (2008) 141-144.
[23] A. Ingle, M. Rai, A. Gade, M. Bawaskar, Fusarium solani: a novel biological agent for the extracellular synthesis of silver nanoparticles, Journal of Nanoparticle Research, 11 (2009) 2079-2085.
[24] K. Kathiresan, S. Manivannan, M. Nabeel, B. Dhivya, Studies on silver nanoparticles synthesized by a marine fungus, Penicillium fellutanum isolated from coastal mangrove sediment, Colloids and surfaces B: Biointerfaces, 71 (2009) 133-137.
[25] N. Durán, P.D. Marcato, G.I. De Souza, O.L. Alves, E. Esposito, Antibacterial effect of silver nanoparticles produced by fungal process on textile fabrics and their effluent treatment, Journal of biomedical nanotechnology, 3 (2007) 203-208.
[26] A. Syed, S. Saraswati, G.C. Kundu, A. Ahmad, Biological synthesis of silver nanoparticles using the fungus Humicola sp. and evaluation of their cytoxicity using normal and cancer cell lines, Spectrochimica Acta Part A: Molecular and Biomolecular Spectroscopy, 114 (2013) 144-147.
[27] A. Ahmad, P. Mukherjee, S. Senapati, D. Mandal, M.I. Khan, R. Kumar, M. Sastry, Extracellular biosynthesis of silver nanoparticles using the fungus *Fusarium oxysporum*, Colloid Surf. B: Biointerf, 28 (2003) 313-318.
[28] A. Chwalibog, E. Sawosz, A. Hotowy, J. Szeliga, S. Mitura, K. Mitura, M. Grodzik, P. Orlowski, A. Sokolowska, Visualization of interaction between inorganic nanoparticles and bacteria or fungi, International Journal of Nanomedicine, 5 (2010) 1085.
[29] R. Sanghi, P. Verma, Biomimetic synthesis and characterisation of protein capped silver nanoparticles, Bioresource technology, 100 (2009) 501-504.
[30] S. Roy, T. Mukherjee, S. Chakraborty, T.K. Das, Biosynthesis, characterisation & antifungal activity of Silver nanoparticles synthesized by the fungus aspergillus Foetidus mtcc8876, Digest Journal of Nanomaterials and Biostructures, 8 (2013) 197-205.
[31] M. Moazeni, A.R. Shahverdi, M. Nabili, F. Noorbakhsh, S. Rezaie, Green synthesis of silver nanoparticles: The reasons for and against Aspergillus parasiticus, Nanomed. J, 1 (2014) 267-275.
[32] A.R. Abd El-Aziz, Eco-friendly biosynthesis of silver nanoparticles by Aspergillus parasiticus, Digest Journal Of Nanomaterials And Biostructures, 9 (2014) 1485.
[33] G. Li, D. He, Y. Qian, B. Guan, S. Gao, Y. Cui, K. Yokoyama, L. Wang, Fungus-mediated green synthesis of silver nanoparticles using Aspergillus terreus, International journal of molecular sciences, 13 (2012) 466-476.
[34] K.S. Siddiqi, A. Husen, Recent advances in plant-mediated engineered gold nanoparticles and their application in biological system, Journal of Trace Elements in Medicine and Biology, 40 (2017) 10-23.
[35] M. Kumari, S. Pandey, V.P. Giri, A. Bhattacharya, R. Shukla, A. Mishra, C. Nautiyal, Tailoring shape and size of biogenic silver nanoparticles to enhance antimicrobial efficacy against MDR bacteria, Microbial pathogenesis, 105 (2017) 346-355.
[36] N. Vigneshwaran, A.A. Kathe, P. Varadarajan, R.P. Nachane, R. Balasubramanya, Biomimetics of silver nanoparticles by white rot fungus, Phaenerochaete chrysosporium, Colloids and Surfaces B: Biointerfaces, 53 (2006) 55-59.
[37] P. Mukherjee, M. Roy, B. Mandal, G. Dey, P. Mukherjee, J. Ghatak, A. Tyagi, S. Kale, Green synthesis of highly stabilized nanocrystalline silver particles by a non-pathogenic and agriculturally important fungus T. asperellum, Nanotechnology, 19 (2008) 075103.
[38] R.M. Elamawi, R.E. Al-Harbi, A.A. Hendi, Biosynthesis and characterization of silver nanoparticles using Trichoderma longibrachiatum and their effect on phytopathogenic fungi, Egyptian Journal of Biological Pest Control, 28 (2018) 28.

[39] R. Al-Bahrani, J. Raman, H. Lakshmanan, A.A. Hassan, V. Sabaratnam, Green synthesis of silver nanoparticles using tree oyster mushroom Pleurotus ostreatus and its inhibitory activity against pathogenic bacteria, Materials Letters, 186 (2017) 21-25.
[40] A. Gliga, S. Skoglund, I. Odnevall Wallinder, B. Fadeel, H. Karlsson, Size-dependent cytotoxicity of silver nanoparticles in human lung cells: the role of cellular uptake, agglomeration and Ag release, Part. Fibre. Toxicol, 11 (2014) 1-17.
[41] A.L. Holder, L.C. Marr, Research Article Toxicity of Silver Nanoparticles at the Air-Liquid Interface, (2013).
[42] X. Han, R. Gelein, N. Corson, P. Wade-Mercer, J. Jiang, P. Biswas, J.N. Finkelstein, A. Elder, G. Oberdörster, Validation of an LDH assay for assessing nanoparticle toxicity, Toxicology, 287 (2011) 99-104.
[43] C. Carlson, S.M. Hussain, A.M. Schrand, K. Braydich-Stolle, K.L. Hess, R.L. Jones, J.J. Schlager, Unique Cellular Interaction of Silver Nanoparticles: Size-Dependent Generation of Reactive Oxygen Species, J. Phys. Chem. B, 112 (2008) 13608-13619.
[44] X. Wang, Z. Ji, C.H. Chang, H. Zhang, M. Wang, Y.P. Liao, S. Lin, H. Meng, R. Li, B. Sun, L.V. Winkle, K.E. Pinkerton, J.I. Zink, T. Xia, A.E. Nel, Use of Coated Silver Nanoparticles to Understand the Relationship of Particle Dissolution and Bioavailability to Cell and Lung Toxicological Potential, Small, 10 (2014) 385-398.
[45] C. Beer, R. Foldbjerg, Y. Hayashi, D.S. Sutherland, H. Autrup, Toxicity of silver nanoparticles—nanoparticle or silver ion?, Toxicology letters, 208 (2012) 286-292.
[46] P. Cronholm, H.L. Karlsson, J. Hedberg, T.A. Lowe, L. Winnberg, K. Elihn, I.O. Wallinder, L. Möller, Intracellular uptake and toxicity of Ag and CuO nanoparticles: a comparison between nanoparticles and their corresponding metal ions, Small, 9 (2013) 970-982.
[47] J.R. Lead, G.E. Batley, P.J. Alvarez, M.N. Croteau, R.D. Handy, M.J. McLaughlin, J.D. Judy, K. Schirmer, Nanomaterials in the environment: behavior, fate, bioavailability, and effects—an updated review, Environmental toxicology and chemistry, 37 (2018) 2029-2063.
[48] M. Sikder, J.R. Lead, G.T. Chandler, M. Baalousha, A rapid approach for measuring silver nanoparticle concentration and dissolution in seawater by UV-vis, NanoImpact (submitted), (2016).
[49] M. Sikder, E. Eudy, G.T. Chandler, M. Baalousha, Comparative study of dissolved and nanoparticulate Ag effects on the life cycle of an estuarine meiobenthic copepod, Amphiascus tenuiremis, Nanotoxicology, 12 (2018) 375-389.
[50] R. MacCuspie, Colloidal stability of silver nanoparticles in biologically relevant conditions, J. Nanopar. Res, 13 (2011) 2893-2908.
[51] G.J. Kenne, P.M. Gummadidala, M.H. Omebeyinje, A.M. Mondal, D.K. Bett, S. McFadden, S. Bromfield, N. Banaszek, M. Velez-Martinez, C. Mitra, I. Mikell, S. Chatterjee, J. Wee, A. Chanda, Activation of Aflatoxin Biosynthesis Alleviates Total ROS in Aspergillus parasiticus, Toxins (Basel), 10 (2018).
[52] M.M. Nabi, J. Wang, M. Meyer, M.-N. Croteau, N. Ismail, M. Baalousha, Concentrations and size distribution of TiO2 and Ag engineered particles in five wastewater treatment plants in the United States, Science of The Total Environment, 753 (2021) 142017.
[53] H.E. Pace, N.J. Rogers, C. Jarolimek, V.A. Coleman, E.P. Gray, C.P. Higgins, J.F. Ranville, Single particle inductively coupled plasma-mass spectrometry: a performance evaluation and method comparison in the determination of nanoparticle size, Environ. Sci. Technol, 46 (2012) 12272-12280.
[54] M. Baalousha, Y. Ju-Nam, P.A. ole, J.A. riljac, I.P. ones, C.R. yler, V. tone, T.F. ernandes, M.A. epson, J.R. ead, Characterization of cerium oxide nanoparticles–Part 2: Nonsize measurements, Environ. Toxicol. Chem, 31 (2012) 994-1003.
[55] P. Hamilton, G. Hockey, M. Rejman, The place of the concept of activation in human information processing theory: An integrative approach, Attention and performance, 6 (1977) 463-486.
[56] G.M. Rand, S.R. Petrocelli, Fundamentals of aquatic toxicology, HEMISPHERE, 1985.
[57] M.R. Eftink, C.A. Ghiron, Fluorescence quenching studies with proteins, Analytical biochemistry, 114 (1981) 199-227.

[58] K.C. Bhainsa, S. D'souza, Extracellular biosynthesis of silver nanoparticles using the fungus Aspergillus fumigatus, Colloids and surfaces B: Biointerfaces, 47 (2006) 160-164.
[59] I. Maliszewska, A. Juraszek, K. Bielska, Green synthesis and characterization of silver nanoparticles using ascomycota fungi Penicillium nalgiovense AJ12, Journal of Cluster Science, 25 (2014) 989-1004.
[60] D. Ballottin, S. Fulaz, M.L. Souza, P. Corio, A.G. Rodrigues, A.O. Souza, P.M. Gaspari, A.F. Gomes, F. Gozzo, L. Tasic, Elucidating Protein Involvement in the Stabilization of the Biogenic Silver Nanoparticles, Nanoscale Research Letters, 11 (2016) 313.
[61] B. Mousavi, F. Tafvizi, S. Zaker Bostanabad, Green synthesis of silver nanoparticles using Artemisia turcomanica leaf extract and the study of anti-cancer effect and apoptosis induction on gastric cancer cell line (AGS), Artificial Cells, Nanomedicine, and Biotechnology, 46 (2018) 499-510.
[62] N.G. Bastús, J. Piella, V. Puntes, Quantifying the Sensitivity of Multipolar (Dipolar, Quadrupolar, and Octapolar) Surface Plasmon Resonances in Silver Nanoparticles: The Effect of Size, Composition, and Surface Coating, Langmuir, 32 (2016) 290-300.
[63] S. Peng, J.M. McMahon, G.C. Schatz, S.K. Gray, Y. Sun, Reversing the size-dependence of surface plasmon resonances, Proceedings of the National Academy of Sciences, 107 (2010) 14530-14534.
[64] M.S. Frost, M.J. Dempsey, D.E. Whitehead, The response of citrate functionalised gold and silver nanoparticles to the addition of heavy metal ions, Colloids and Surfaces A: Physicochemical and Engineering Aspects, 518 (2017) 15-24.
[65] M. Baalousha, Y. Ju-Nam, P.A. Cole, B. Gaiser, T.F. Fernandes, J.A. Hriljac, M.A. Jepson, V. Stone, C.R. Tyler, J.R. Lead, Characterization of cerium oxide nanoparticles–Part 1: Size measurements, Environ. Toxicol. Chem, 31 (2012) 983-993.
[66] S. Honary, F. Zahir, Effect of Zeta Potential on the Properties of Nano-Drug Delivery Systems-A Review (Part 2), Tropic. J. Pharmaceut. Res, 12 (2013) 265-273.
[67] G.V. Lowry, R.J. Hill, S. Harper, A.F. Rawle, C.O. Hendren, F. Klaessig, U. Nobbmann, P. Sayre, J. Rumble, Guidance to improve the scientific value of zeta-potential measurements in nanoEHS, Environmental Science: Nano, 3 (2016) 953-965.
[68] A.K. Ostermeyer, C. Kostigen Mumuper, L. Semprini, T. Radniecki, Influence of Bovine Serum Albumin and Alginate on Silver Nanoparticle Dissolution and Toxicity to Nitrosomonas europaea, Environ. Sci. Technol, 47 (2013) 14403-14410.
[69] X. Li, K. Schirmer, L. Bernard, L. Sigg, S. Pillai, R. Behra, Silver nanoparticle toxicity and association with the alga Euglena gracilis, Environmental Science: Nano, 2 (2015) 594-602.
[70] Z.M. Xiu, Q.b. Zhang, H.L. Puppala, V.L. Colvin, P.J.J. Alvarez, Negligible Particle-Specific Antibacterial Activity of Silver Nanoparticles, Nano Lett, 12 (2012) 4271-4275.
[71] A.-J. Miao, Z. Luo, C.-S. Chen, W.-C. Chin, P.H. Santschi, A. Quigg, Intracellular Uptake: A Possible Mechanism for Silver Engineered Nanoparticle Toxicity to a Freshwater Alga *Ochromonas danica*., PLoS One, 5 (2011) e15196-15191-e15196-15198.
[72] D.E. Gorka, J. Liu, Effect of Direct Contact on the Phytotoxicity of Silver Nanomaterials, Environmental Science & Technology, 50 (2016) 10370-10376.
[73] J. Wu, Q. Yu, T. Bosker, M.G. Vijver, W.J. Peijnenburg, Quantifying the relative contribution of particulate versus dissolved silver to toxicity and uptake kinetics of silver nanowires in lettuce: impact of size and coating, Nanotoxicology, (2020) 1-16.
[74] L. Li, H. Wu, W.J. Peijnenburg, C.A. van Gestel, Both released silver ions and particulate Ag contribute to the toxicity of AgNPs to earthworm Eisenia fetida, Nanotoxicology, 9 (2015) 792-801.
[75] Z. Huang, P. Xu, G. Chen, G. Zeng, A. Chen, Z. Song, K. He, L. Yuan, H. Li, L. Hu, Silver ion-enhanced particle-specific cytotoxicity of silver nanoparticles and effect on the production of extracellular secretions of Phanerochaete chrysosporium, Chemosphere, 196 (2018) 575-584.

627 **Table 1.** Sizes and zeta potential of AgNPs.

AgNPs	Z-average (nm) DLS*	PdI	Hydrodynamic diameter FFF**	Core size sp-ICP-MS	TEM**	Zeta potential
np-AgNPs	132.0 ± 2.0	0.6 ± 0.0	ND	ND	74.1 ± 19.7	-31.4 ± 0.7
Cit-AgNPs	21.5 ± 0.1	0.1 ± 0.0	11.3 ± 8.7	22.6 ± 2.9	9.7 ± 3.5	-42.1 ± 1.6
CFE:$AgNO_3$ (50:1)	38.6 ± 0.1	0.2 ± 0.0	26.3 ± 16.6	25.3 ± 10.9	15.9 ± 6.4	-42.0 ± 1.1
(25:1)	79.1 ± 0.8	0.3 ± 0.0	26.2 ± 17.8	26.8 ± 7.3	ND	-38.7 ± 1.1
(10:1)	34.4 ± 0.6	0.4 ± 0.1	23 ± 14.6	31.9 ± 11.9	ND	-37.8 ± 1.8
(5:1)	104.2 ± 60.3	0.3 ± 0.0	41.2 ± 24.4	29.3 ± 16.4	ND	-27.2 ± 2.5
(1:1)	72.8 ± 5.6	0.6 ± 0.1	49.8 ± 21.1	26.4 ± 7.9	ND	-24.5 ± 2.8
(1:5)	157.3 ± 17.7	0.5 ± 0.1	29.5 ± 20.1	23.4 ± 7.9	ND	-28.6 ± 3.1
(1:10)	182.4 ± 49.2	0.5 ± 0.1	36.0 ± 20.7	24.3 ± 8.4	ND	-25.2 ± 2.6

628 ± represent the standard deviation of the measurement, not the standard deviation of size distribution.

629 * The standard deviation is that of replicates

630 ** The standard deviation is that of the size distribution

631

632

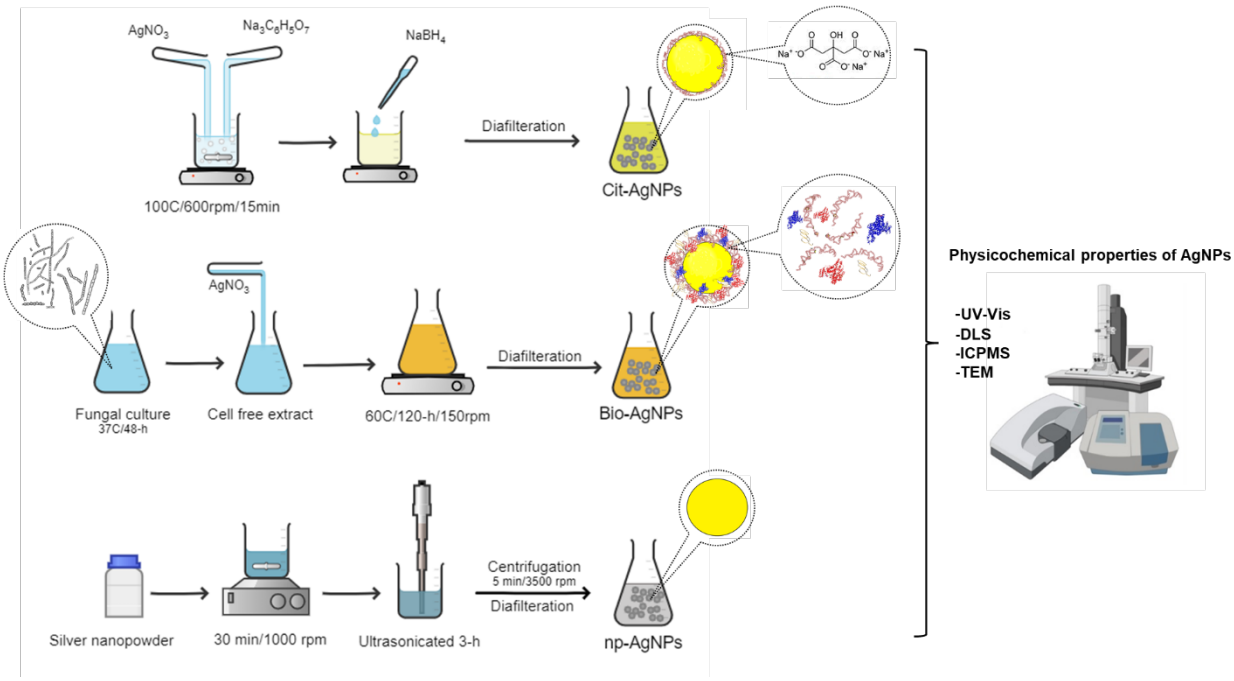

Figure 1. Schematic representation of the chemical and biological synthesis, as well as the nanopowder dispersion.

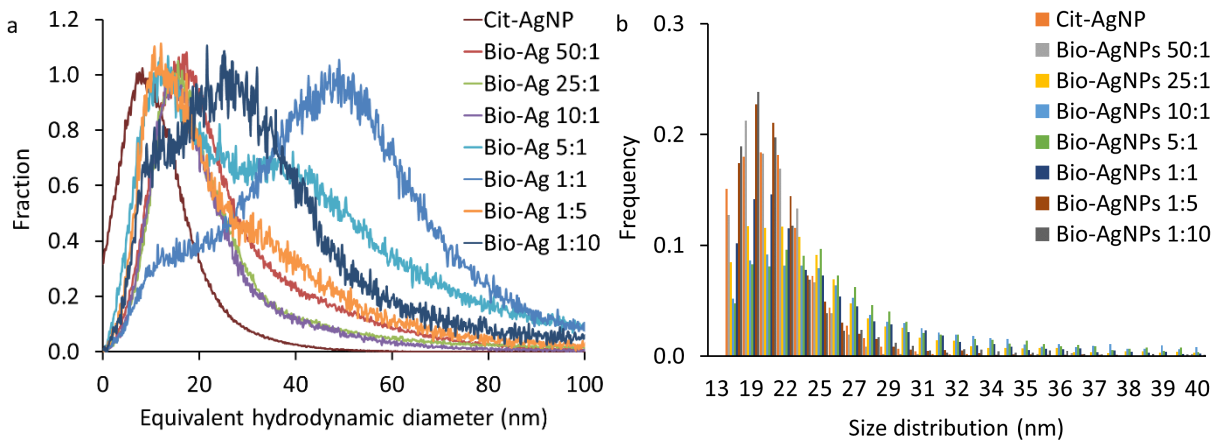

639

640 **Figure 2.** Particle size distribution of cit-AgNPs and bio-AgNPs: (a) equivalent hydrodynamic diameter
641 measured by asymmetrical flow-field flow fractionation coupled with an inductively coupled plasma-mass
642 spectrometer (AF4-ICP-MS), and (b) number particle size distribution measured by single particle-
643 inductively coupled plasma-mass spectrometer (SP-ICP-MS). Bio-AgNPs were produced by varying cell
644 free extract:$AgNO_3$ ratio (50:1, 25:1, 10:1, 5:1, 1:1, 1:5 and 1:10). Reaction conditions: $[Ag^+] = 10^{-3}$ M,
645 incubation temp = 60 °C.

646

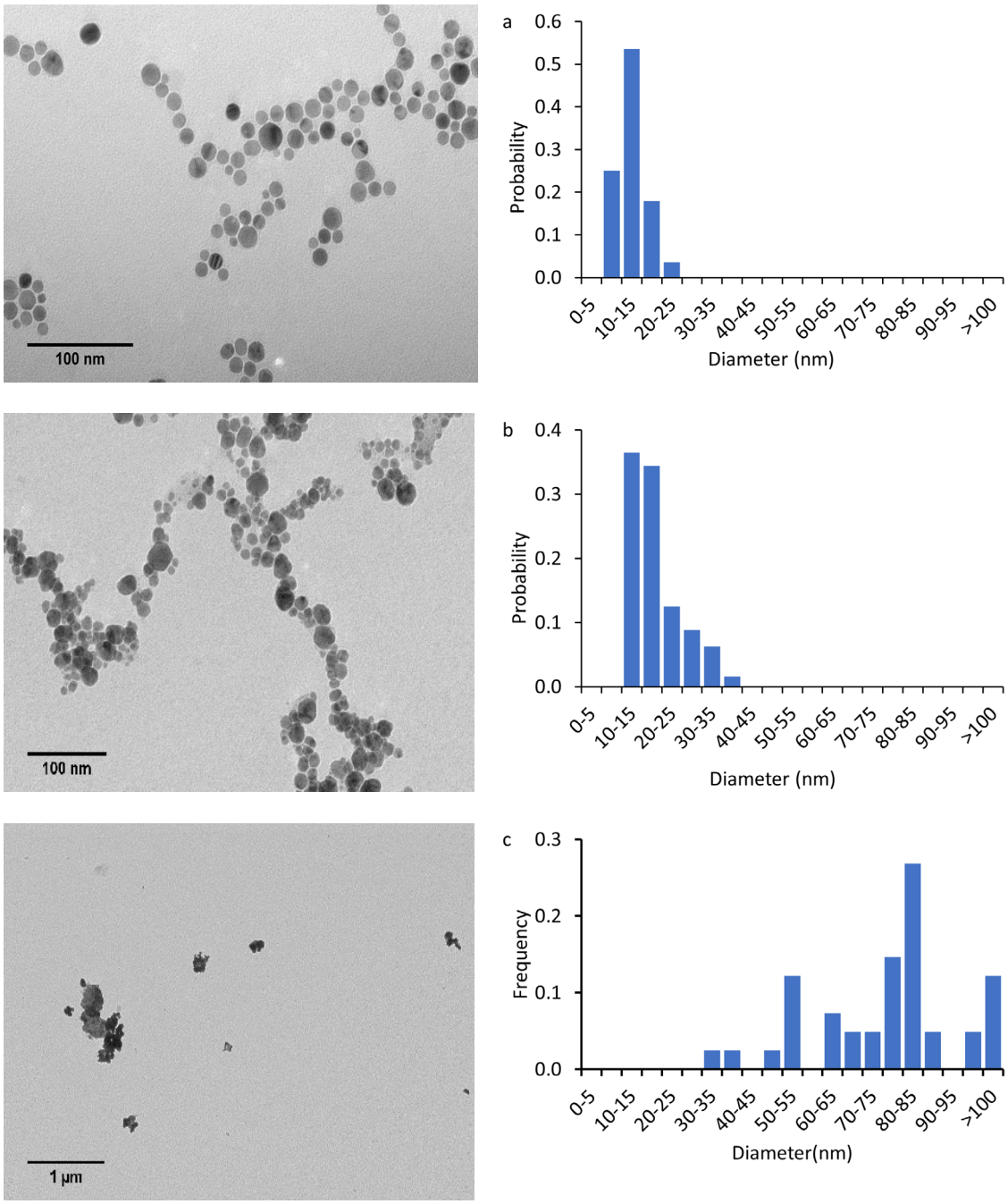

Figure 3. Representative transmission electron microscopy micrographs of (a) chemically synthesized silver nanoparticles cit-AgNPs, (b) biologically synthesized silver nanoparticles (bio-AgNPs), and (c) commercially available silver nanopowders (np-AgNPs).

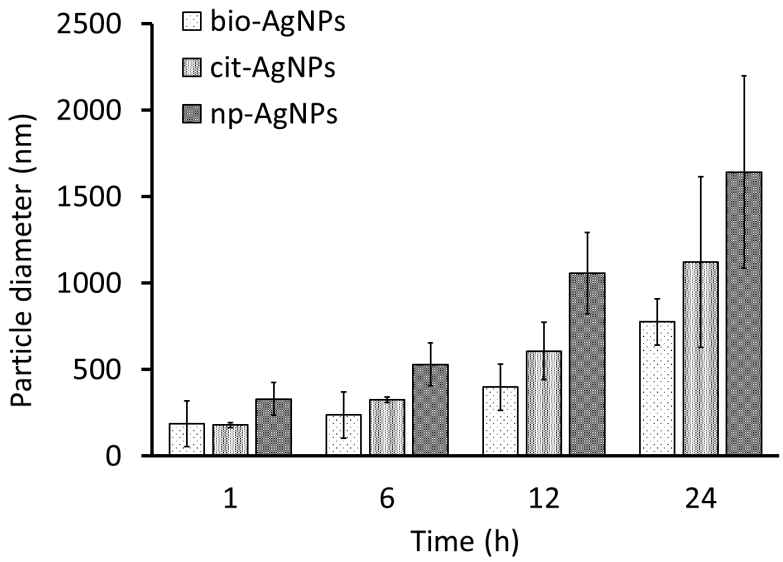

650

651 **Figure 4.** Aggregation of AgNPs in seawater during the exposure measured by dynamic light scattering.

652

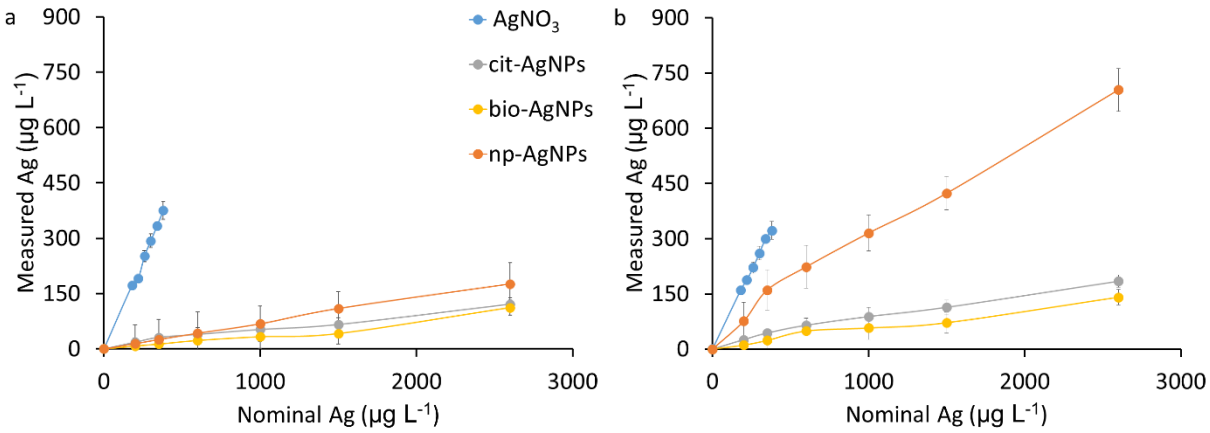

653

654 **Figure 5**. Dissolved Ag concentrations in the seawater at (a) the beginning (0 h) and (b) end of the exposure

655 (24 h).

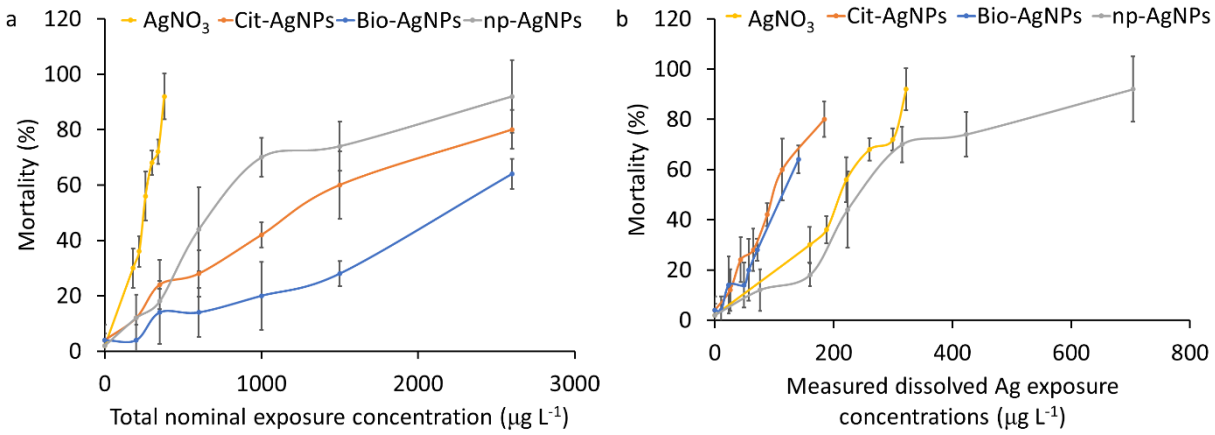

656

657 **Figure 6.** Toxicity (mortality) in the juvenile clams *Mercenaria Mercenaria* after 24 h acute exposure to
658 dissolved and particulate Ag as a function of (a) total nominal exposure concentration, and (b) measured
659 dissolved Ag exposure concentration.